O.V. PYLYPOVSKYI,[1] D.D. SHEKA,[1] V.P. KRAVCHUK,[2] YU.B. GAIDIDEI,[2] F.G. MERTENS[3]

[1] Taras Shevchenko National University of Kyiv
(60, Volodymyrs'ka Str., 01601 Kyiv, Ukraine; e-mail: engraver@univ.net.ua)
[2] Bogolyubov Institute for Theoretical Physics, Nat. Acad. of Sci. of Ukraine
(14b, Metrolohichna Str., Kyiv, 03680, Ukraine)
[3] Physics Institute, University of Bayreuth
(95440 Bayreuth, Germany)

UDC 539

MECHANISM OF FAST AXIALLY SYMMETRIC REVERSAL OF MAGNETIC VORTEX CORE

The magnetic vortex core in a nanodot can be switched by an alternating transversal magnetic field. We propose a simple collective coordinate model, which describes the comprehensive vortex core dynamics, including the resonant behavior, weakly nonlinear regimes, and reversal dynamics. A chaotic dynamics *of the vortex polarity is predicted. All analytical results are confirmed by micromagnetic simulations.*

K e y w o r d s: magnetic vortex, nanodot, nanodisk, vortex random-access memories.

1. Introduction

Manipulation of complex magnetization configurations on the scales of nanometers and picoseconds is crucial for the physics of nanomagnetism [1]. Among the variety of different topologically nontrivial configurations, the vortex configuration attracts a special interest: it can form a ground state of micro- and nanosized disk-shaped particles (nanodisks). A magnetic vortex is characterized by an in-plane curling flux – closed structure, which minimizes the magnetostatic energy of a particle, and the out-of-plane region of the vortex core with about the size of the exchange length (typically about 10 nm for magnetically soft materials [2]), which appears due to the dominant role of exchange interaction inside the core [3]. The direction of the vortex core magnetization, the so-called vortex polarity $p = \pm 1$ (up or down), can be considered as a bit of information in the nonvolatile magnetic vortex random-access memories (VRAM) [4, 5]. To realize the concept of VRAM, one needs to control the vortex polarity switching process in a fast way.

There exist different ways to switch the vortex polarity. One can distinguish two basic scenarios of the switching: (i) Axially asymmetric switching occurs, e.g. under the action of different in-plane AC magnetic fields or by a spin polarized current, see Ref. 6 and references therein. Such a switching occurs due to the nonlinear resonance in the system of certain magnon modes with nonlinear coupling [7, 8], which is accompanied by the temporary creation and annihilation of vortex-antivortex pairs. (ii) The axially symmetric (or punch-through) switching occurs, e.g., under the influence of a DC transversal field [9–12]. The mechanism of such a switching is the direct pumping of axially symmetric magnon modes. Very recently, the resonant pumping of such modes by an AC transversal field was proposed to switch the vortex in micromagnetic simulations [13, 14], which gives a possibility to achieve a switching at much lower field intensities.

The aim of the current study is to develop a theory for the axially symmetric vortex polarity switching. We propose a simple analytical *two-parameter cutoff model*, which allows us to describe the main features of the complicated vortex dynamics under the action of AC pumping, including a nonlinear resonance and the magnetization reversal. Our model predicts a *chaotic dynamics* of the vortex polarity, which is analyzed in terms of Poincaré maps. Our full-scale micromagnetic simulations confirmed all analytical predictions.

2. Two–Parameter Cutoff Model

We consider the model of a classical 2D Heisenberg ferromagnet with effective easy-plane anisotropy,

caused by the dipolar interaction, under the action of a transversal AC field. The energy of such a magnet normalized by the value πA, with A being the exchange constant, reads

$$E = \frac{1}{2}\int W \mathrm{d}^2x,$$
$$W = \frac{(\boldsymbol{\nabla} m)^2}{1-m^2} + \left(1-m^2\right)(\boldsymbol{\nabla}\phi)^2 + \frac{m^2}{\ell^2} - \frac{2mh(\tau)}{\ell^2}. \quad (1)$$

Here, m and ϕ are related to the components of the magnetization vector

$$\mathbf{M} = M_S(\sqrt{1-m^2}\cos\phi, \sqrt{1-m^2}\sin\phi, m),$$

the parameter $\ell = \sqrt{A/4\pi M_S^2}$ is the exchange length, M_S is the saturation magnetization, and $h(\tau) = h\sin\omega\tau$ is the dimensionless external AC field. We use here the dimensionless time $\tau = \Omega_0 t$ with $\Omega_0 = 4\pi\gamma_0 M_S$, with γ_0 being the gyromagnetic ratio. The magnetization dynamics follows the Landau–Lifshitz equations, which can be derived from the Lagrangian

$$L = G - E, \quad G = \frac{1}{2\pi\ell^2}\int \mathrm{d}^2x\,(1-m)\,\dot{\phi} \quad (2)$$

and the dissipation function

$$F = \frac{\eta}{2\pi\ell^2}\int \mathrm{d}^2x\left[\frac{\dot{m}^2}{1-m^2} + (1-m^2)\dot{\phi}^2\right]. \quad (3)$$

Here and below, the overdot means the derivative with respect to τ, and the parameter η is the Gilbert damping coefficient.

In order to describe the switching phenomena, we propose a simple analytical picture, by using the following two-parameter ansatz for the magnetization variables:

$$m(r,\tau) = \mu(\tau) f\left(\frac{r}{\ell}\right),\ \phi(r,\tau) = \chi \pm \frac{\pi}{2} + \psi(\tau) g\left(\frac{r}{\ell}\right). \quad (4)$$

We consider the vortex core amplitude $m(0,\tau) = \mu(\tau)$, whose direction has the sense of the *dynamical vortex polarity* and is considered as a collective variable together with the in-plane *turning phase* $\psi(\tau)$, and the functions $f(x)$ and $g(x)$ describe the vortex structure. We use a Gaussian distribution for both functions, $f(x) = g(x) = \exp(-x^2/2)$, which is in a good agreement with simulation data. One has to note that such an ansatz describes an axially symmetric vortex solution together with the simplest axially symmetric magnon mode: the real solution just slightly varies the profile of the functions $f(x)$ and $g(x)$. It is also possible to take higher modes (with additional nodes on r) into account, but we try to make the picture as simple as possible.

Using this ansatz, one can calculate the total energy of the vortex state disk as follows:

$$E = \int_a^R W r \mathrm{d}r = \ln\frac{R}{a} + \mathcal{E}(\mu,\psi).$$

Here, R is the disk radius, and a is a cutoff parameter, which is of order of the magnetic lattice constant a_0. We introduce here the cutoff in order to take discreteness effects into account. It is worth to recall that, in the continuum theory, two vortex states with different polarities are separated by an infinite barrier which prohibits the switching in a simply connected domain. The function $\mathcal{E}(\mu,\psi)$ is the effective energy of the system:

$$\mathcal{E} = \frac{\varkappa\mu^2}{2} + \frac{1}{2}\mathrm{Li}_2(\mu^2) + \frac{\psi^2}{2} - \frac{\mu^2\psi^2}{8} - 2h\mu\sin\omega\tau. \quad (5)$$

Here, $\mathrm{Li}_2(x)$ is a dilogarithm function [15], $\varkappa = \ln\lambda + \gamma + 1$, with $\gamma \approx 0.577$ being Euler's constant, and we assume that $\lambda = a^2/\ell^2 \ll 1$.

The effective Lagrangian and dissipation functions take the following forms:

$$\mathcal{L} = -\frac{1}{2}\mu\dot{\psi} - \mathcal{E},$$
$$\mathcal{F} = \frac{\eta}{2}\left[-\frac{\dot{\mu}^2}{\mu^2}\ln\left(1-\mu^2\right) + \dot{\psi}^2 - \frac{1}{2}\mu^2\dot{\psi}^2\right]. \quad (6)$$

The effective equations of motion are then obtained as the Euler–Lagrange equations

$$\frac{\partial\mathcal{L}}{\partial X_i} - \frac{\mathrm{d}}{\mathrm{d}\tau}\frac{\partial\mathcal{L}}{\partial\dot{X}_i} = \frac{\partial\mathcal{F}}{\partial\dot{X}_i}, \quad X_i = \{\mu,\psi\}, \quad (7)$$

which finally read:

$$\dot{\psi} = -2\varkappa\mu + \frac{1}{2}\mu\psi^2 + \frac{2}{\mu}\ln(1-\mu^2) + 4h\sin\omega\tau + 2\eta\frac{\dot{\mu}}{\mu^2}\ln(1-\mu^2), \quad (8a)$$
$$\dot{\mu} = -\frac{1}{2}\psi\left(\mu^2-4\right) - \eta(\mu^2-2)\dot{\psi}. \quad (8b)$$

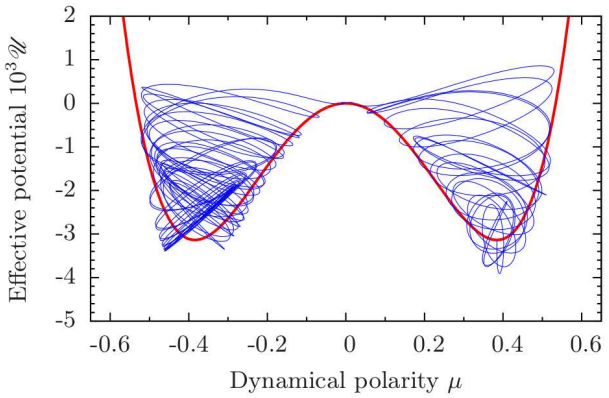

Fig. 1. Effective double-well potential $\mathcal{U}(\mu)$, see (9) (solid line). The cutoff parameter $\lambda = 0.07$. The typical evolution of the energy as a function of the dynamical polarity $\mu(\tau)$ under the periodic pumping for unidirectional switching is shown by the thin line as a result of the numerical integration of Eqs. (8). System parameters: $h = 0.001$ with frequency $\omega = 0.7547$, damping $\eta = 0.001$, initial conditions $\mu(\tau = 0) = \mu_0 = 0.384$, $\psi(\tau = 0) = 0$, integration time $\tau_{\text{all}} = 5000$, the trajectory is shown till $\tau_{\text{sh}} = 500$

We start with the case without damping, $\eta = 0$. In this case, one can easily exclude the turning phase ψ from the consideration, which results in the following effective Lagrangian for the dynamical polarity only:

$$\mathcal{L}^{\text{ef}} = \frac{1}{2}\mathcal{M}(\mu)\dot{\mu}^2 - \mathcal{U}(\mu) + 2\mu h \sin\omega\tau,$$
$$\mathcal{M}(\mu) = \frac{1}{4-\mu^2}, \quad \mathcal{U}(\mu) = \frac{\varkappa\mu^2}{2} + \frac{1}{2}\text{Li}_2\left(\mu^2\right). \tag{9}$$

The Lagrangian (9) describes the motion of a particle with the variable mass $\mathcal{M}(\mu)$ in a double-well potential $\mathcal{U}(\mu)$ under the action of a periodic pumping. The typical shape of the potential $\mathcal{U}(\mu)$ is shown in Fig. 1: it has two energetically equivalent ground states with $\mu = \pm\mu_0$, which correspond to vortices with opposite polarities. In our cutoff model, μ_0 is a nonzero solution of the transcendent equation:

$$\varkappa\mu_0^2 = \ln\left(1-\mu_0^2\right). \tag{10}$$

For $\lambda = 0.07$, the energy minimum corresponds to $\mu_0 = 0.384$, see Fig. 1. One has to note that our model works only for $|\mu| < 1$. Another method is to work with a trigonometric variable, the vortex core angle ϑ, instead of the dynamical polarity $\mu = \cos\vartheta$. We checked that the usage of ϑ provides the same physical picture, but the effective equations look awkward, so we keep to work with μ.

The dynamical polarity $\mu(\tau)$ satisfies the following equation (see (9)):

$$\ddot{\mu} + \mathcal{M}\mu\dot{\mu}^2 + \frac{\varkappa\mu}{\mathcal{M}} - \frac{\ln(1-\mu^2)}{\mathcal{M}\mu} = \frac{2h}{\mathcal{M}}\sin\omega\tau. \tag{11}$$

The linear oscillations near the potential well bottom have the usual harmonic shape

$$\mu = \mu_0 + ae^{i\omega_0\tau}, \quad \omega_0 = \sqrt{\frac{2\left(1+\varkappa-\varkappa\mu_0^2\right)}{\mathcal{M}_0(1-\mu_0^2)}}, \quad |a| \ll 1, \tag{12}$$

with $\mathcal{M}_0 = 1/(4-\mu_0^2)$ being the effective mass of a small oscillating particle near the well bottom, and ω_0 being the eigenfrequency.

Let us study the weakly nonlinear dynamics, by using the method of multiple scales [16–18]. We limit ourselves by the three-scale expansion as follows:

$$\mu = \mu_0 + \sum_{n=1}^{3}\varepsilon^n\mu_n(T_0, T_1, T_2), \quad T_n = \varepsilon^n t,$$
$$\omega = \omega_0 + \varepsilon^2\omega_2, \quad h = \varepsilon^3 h_3 \ll 1, \tag{13}$$

which provides a weakly nonlinear expansion to be valid under the condition that the field amplitude is much less than the frequency detuning, $h/(\omega-\omega_0) \ll \ll 1$. Equation (11) together with expansion (13) results in the system of equations for μ_n, see Appendix A for details. Following the Floquet theory [17], one has to remove the mixed-secular terms in such equations, which finally provides the nonlinear resonant curve (see Appendix A for details):

$$\omega_\pm(|a|) = \omega_0 - c_1|a|^2 \pm c_2\frac{h}{|a|}, \tag{14}$$

where $|a|$ is the amplitude of oscillations, see (12), and the parameters c_1 and c_2 are calculated in (A3). A typical nonlinear resonance curve is plotted in Fig. 2. The low-frequency branch ω_- contains a shock-stalling region. The upper limit of such an instability region can be found using the condition $\partial\omega_-/\partial a = 0$, which finally results in the limit frequency

$$\omega_{\text{u}} = \omega_0 - 3\left(\frac{\sqrt{c_1}c_2 h}{2}\right)^{2/3}. \tag{15}$$

The unstable part of the resonance curve is plotted in Fig. 2 by the dash-dotted line. A further increase

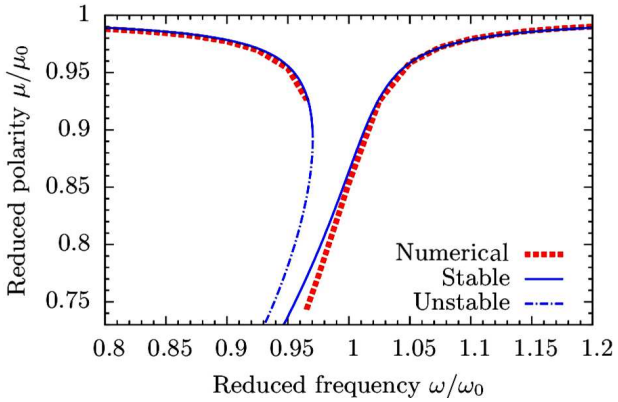

Fig. 2. Nonlinear resonance: amplitude-frequency characteristics from a numerical solution of Eqs. (8) (dashed curve) with initial conditions $\mu(\tau = 0) = \mu_0$ and $\psi(\tau = 0) = 0$. The cutoff parameter $\lambda = 0.07$, the damping $\eta = 0.001$. The thin curves correspond to the analytical solution (14) without damping: the solid lines correspond to the stable solution and the dash-dotted line corresponds to the unstable region (15). The field amplitude $h/\eta = 0.15$. The total computation time for each point $\tau_{\text{tot}} = 3000$

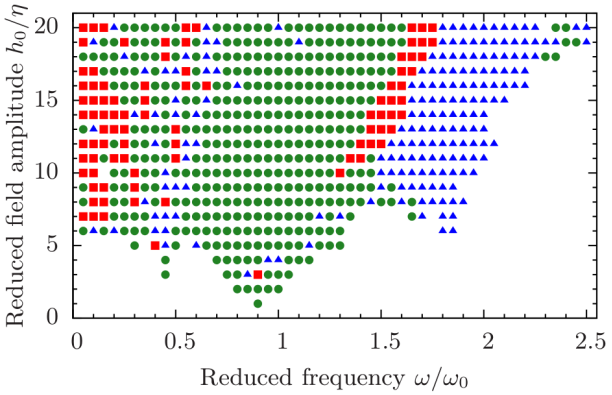

Fig. 3. Diagram of dynamical regimes for the field parameters (amplitude and frequency) as a numerical solution of Eqs. (8): circles correspond to one-period oscillations, triangles correspond to multiple-periods oscillations, and squares correspond to chaotic dynamics. White domains correspond to the absence of switching. Parameters are the same as in Fig. 2 (the total computation time τ_{tot} depends on the regime, see the main text)

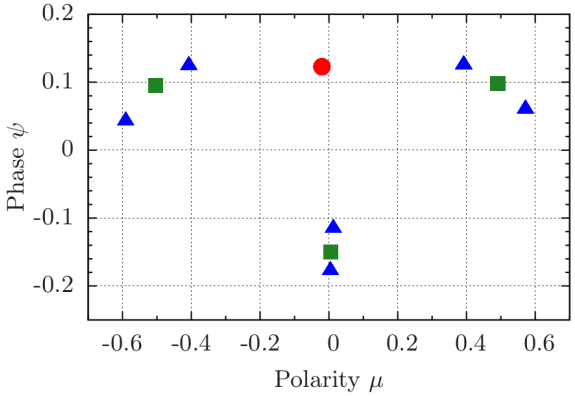

Fig. 4. Poincaré map for regular oscillations. The circle corresponds to $h/\eta = 5$, $\omega/\omega_0 = 0.7$, triangles correspond to $h/\eta = 11$, $\omega/\omega_0 = 2$, and squares correspond to $h/\eta = 13$, $\omega/\omega_0 = 1.95$. Parameters are the same as in Fig. 2

in the field amplitude leads to a broader instability domain. Moreover, we will see below that a stronger pumping results in an essentially different kind of dynamics, leading to the vortex polarity switching and the chaotic behavior.

If we increase the forcing amplitude, the system goes to a strongly nonlinear regime. We analyze such regimes using numerical solutions of Eqs. (8). First of all, the regular oscillations of the dynamical polarity $\mu(\tau)$ between two potential wells occur in a wide range of parameters (the typical oscillations $\mathcal{U}(\mu)$ are plotted by the thin curve in Fig. 1). The diagram of dynamical regimes is shown in Fig. 3. Different types of dynamical regimes are classified in accordance to the Poincaré maps. These maps are constructed for 20 000 periods of the field oscillations for frequencies greater than $0.6\omega_0$ and for 15 000 oscillation periods for other frequencies. The first 5000 points are dropped from consideration in order to exclude transient processes. The diagram of dynamical regimes has a resonant behavior at the frequencies $\omega_0/3$, $\omega_0/2$, ω_0, and $2\omega_0$, see Fig. 3.

There are three different dynamical regimes on the diagram:

(i) One-period oscillations (circles in Fig. 3) occur in a wide range of parameters, generally in a vicinity of the resonance frequency ω_0, the Poincaré map for this regime has one stable focus (a circle in Fig. 4).

(ii) Multiple-period oscillations (triangles in Fig. 3) occur typically near the doubled resonance frequency; the Poincaré map has a few points which are attended every pumping period, and the trajectory in phase space (μ, ψ) makes a few windings before closing, see Fig. 4.

(iii) Chaotic oscillations of the dynamical polarity μ (squares in Fig. 3) take place in the transition region

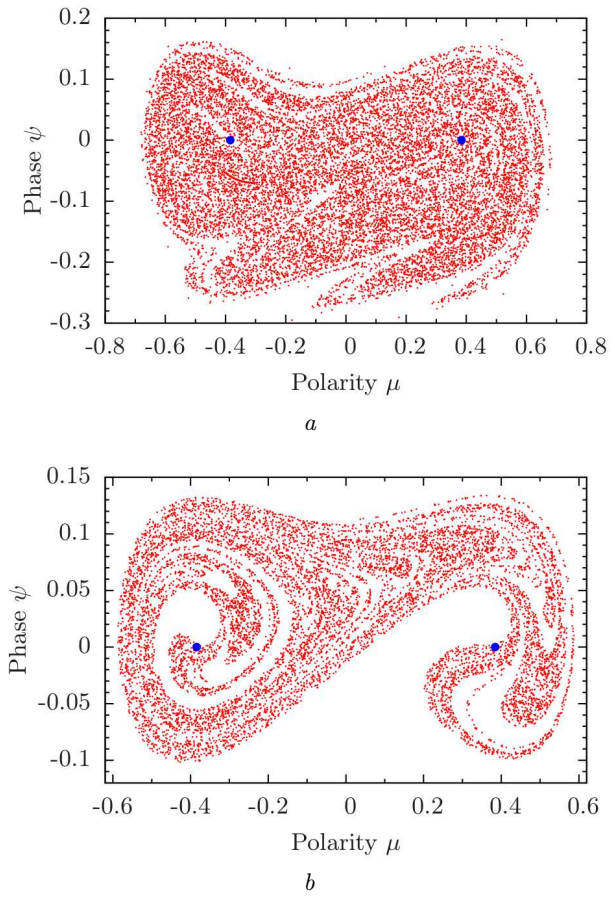

Fig. 5. Strange attractors on the Poincaré map. Equilibrium polarities are marked by circles: $h/\eta = 11$, $\omega/\omega_0 = 1.4$, 15 000 points (a); $h/\eta = 15$, $\omega/\omega_0 = 0.1$, 10 000 points (b)

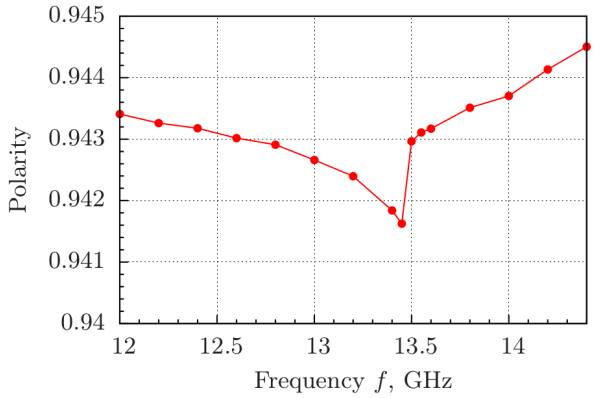

Fig. 6. Instability domain near the first resonance frequency for simulations with the field amplitude 5 mT. The region near the first axially symmetric harmonic is shown

between the oscillations of types (i) and (ii). The corresponding Poincaré map has the shape of a strange attractor, see Fig. 5, *a*. Apart them, the chaotic dynamics occurs at the resonance frequency, the weak enough field amplitude, and in a wide range of the low frequency pumping. The low-frequency dynamics also corresponds to a strange attractor, a typical picture being presented in Fig. 5, *b*.

3. Numerical Study of Different Dynamical Regimes

In order to check all predictions of the two-parameter cutoff model, we performed a full-scale numerical modeling using the OOMMF framework [19], which simulates the Landau–Lifshitz equations. Numerically, we modeled a cylinder-shaped sample with the radius $R = 99$ nm and the height $L = 21$ nm, by using the material parameters for permalloy ($Ni_{80}Fe_{20}$): exchange constant $A = 26$ pJ/m, saturation magnetization $M_S = 860$ kA/m, and Gilbert damping coefficient $\alpha = 0.01$. The two-dimensional space mesh $3 \times 3 \times 21$ nm is used. Initially, the vortex has the upward polarity and the counter-clockwise chirality.

The conditions of our numerical experiment were similar to those in simulations in Wang and Dong [13] and Yoo *et al.* [14]. However, our task was to check the *new* dynamical regime of the *chaotic dynamics*. That is why we need to study the long-time dynamics.

First, we examined the resonant frequency of radial spin waves. A 30-mT constant pulse during 100 ps was applied to the sample; it excited low-amplitude spin waves. By analysis of the Fourier spectrum for a 3.7-ns long-time dynamics of the total magnetization along the disk axis, we calculated the eigenfrequency of the lowest spin wave mode to equal $f_0 = 14$ GHz.

We study the vortex dynamics under the action of a sinusoidal magnetic field

$$\mathbf{B}(t) = \mathbf{e}_z B \sin 2\pi f t \tag{16}$$

directed perpendicularly to the face surfaces of the sample. The vortex dynamics under such a field has a resonant behavior. The weak pumping causes the resonance at the frequency f_0. If we increase the field amplitude, the system goes to a nonlinear regime. The weakly nonlinear regime corresponds to the nonlinear resonance, see Fig. 6 (the resonance on the first axially symmetric harmonic).

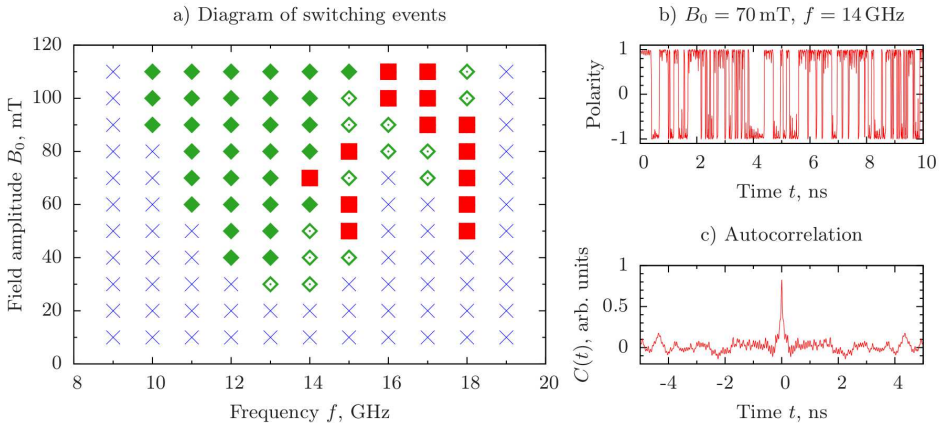

Fig. 7. Numerical simulations of the vortex dynamics: the diagram of dynamical regimes for the field parameters (amplitude and frequency). Diamonds and squares correspond to the switching events (the filled diamonds mark parameters, where the vortex rapidly moves away from the origin after a few switchings, the open diamonds mark the vortex which does not change its position); the filled squares show parameters for the chaotic polarity dynamics, and the crosses correspond to the region without switching events (*a*). Example of the chaotic dynamics for the applied field amplitude $B = 70$ mT and the frequency $f = 14$ GHz (*b*). Autocorrelation function for the plot (*c*)

To systemize the complicated dynamics of the vortex polarity, we compute the phase diagram of the switching events, by varying the field frequency in a vicinity of f_0 from 9 to 19 GHz with steps of 1 GHz and the field amplitude from 10 to 110 mT, see Fig. 7. There are two strong resonances in this range, which agree with the previous results [13,14]. The lower resonance frequency is located between 12 and 14 GHz; it corresponds to the axially symmetric mode without radial nodes ($m = 0$, $n = 0$). The second resonance is located near 18 GHz; it corresponds to the axially symmetric mode with a single radial node ($m = 0$, $n = 1$). Since we expect a chaotic dynamics, it is necessary to analyze the long-time behavior: numerically, we checked the magnetization state every picosecond during the 10-ns interval. The chaotic vortex polarity dynamics during this time is observed in 14 simulations (see filled squares in Fig. 7, *a*, where the vortex polarity switching mechanism corresponds to the axially symmetric way. The typical shape of oscillations is presented in Fig. 7, *b* for $B = 70$ mT and $f = 14$ GHz. We examine the character of the polarity oscillations by an autocorrelation function

$$C(t_i) = \frac{1}{N}\sum_j \mu(t_{i+j})\mu(t_j), \quad i,j = \overline{1,N}, \tag{17}$$

where the discretized time t_n with steps $\Delta t = t_{n+1} - t_n = 1$ ps are used, and $N = 10^4$ is the number of snapshots. The function $\mu(t_i)$ is the discrete dynamical polarity, which is defined as the average magnetization of four cells at the center of the vortex core, normalized by the magnetization in the absence of a forcing. For a chaotic signal, $C(t)$ rapidly decays, see Fig. 7, *c*. We marked points on the diagram of switching events by filled squares for simulations, where the autocorrelation function rapidly decays and the distance between the maximum of the autocorrelation function and the first zero is smaller than 1 ns. Plots of $C(t)$ for other simulations with chaotic dynamics look similarly.

In all simulations, the set of first switchings occurs during the first nanosecond and is accompanied by a high-amplitude axially symmetric spin wave radiation. However, typically, the vortex position at the origin is unstable: during the field pumping, the higher axially nonsymmetric modes ($m \neq 0$) can be excited, which causes a vortex motion toward the disk edge surface. In such a case, the switching occurs through the axially *asymmetric* mechanism, which is accompanied by the temporary creation and annihilation of a vortex-antivortex pair, see Ref. 6 and references therein. Such switching events are shown in Fig. 7, *a* by the filled diamonds. We do not analyze them due to an insufficiently short time interval, compared to the relaxation time, which corresponds to the axially symmetric switching scenario discussed in this work.

4. Conclusions

The axially symmetric vortex polarity switching is an efficient way for the magnetization reversal on a subnanosecond time scale. Very recently, such a scheme was realized by the micromagnetic simulations in Refs. [13, 14]. To gain some insight to the resonant switching effect, the exchange field inside the vortex core was computed in Wang and Dong [13]: it changes rapidly during the vortex reversal. Yoo *et al.* [14] noticed that the switching occurs only if the exchange energy exceeds a threshold value. The crucial role of the exchange interaction becomes clear in the analytical approach developed in the current study. Our two-parameter cutoff model explains the switching phenomenon in terms of the nonlinear resonance in a double-well potential. Such a potential arises mainly from the exchange interaction: the presence of two wells corresponds to the energy degeneracy with respect to the direction of the vortex polarity (up or down); the energy barrier between the wells becomes higher as the discreteness effects become less important.

In terms of our model, the switching can be considered as the motion of an effective mechanical particle with variable mass in a double-well potential. Under the action of a periodic pumping, the particle starts to oscillate near the bottom of one of the wells. When the pumping increases, there appear nonlinear oscillations of the particle; under a further forcing, the particle overcomes the barrier, which corresponds to the magnetization reversal process. The system demonstrates both regular and chaotic dynamics. Very recently, the observation of a chaotic dynamics was reported by Petit–Watelot *et al.* [20] for a spin-current-driven dynamics. It is linked to the commensurability of frequencies in vortex oscillations. In our case, the chaotic dynamics of the magnetization is an analogue of chaotic oscillations, e.g., in a Duffing oscillator [18].

In summary, we analyze analytically and numerically the axially symmetric scenario of the vortex polarity switching induced by an alternating magnetic field directed perpendicularly to the nanodot surface. We propose a simple analytical two-parameter cutoff model, which describes the vortex polarity dynamics under such a resonance pumping and shows the possibility of both periodic and chaotic polarity oscillations by Poincaré maps. The micromagnetic simulations for permalloy confirm a variety of the dynamical regimes and confirm our analytical predictions.

O.V.P. and D.D.S. thank the University of Bayreuth, where a part of this work was performed, for kind hospitality. O.V.P. acknowledges the support from the BAYHOST project. D.D.S. acknowledges the support from the Alexander von Humboldt Foundation.

APPENDIX A.
Analysis by the Method of Multiple Scales

We use the method of multiple scales [16–18] to treat analytically Eq. (11). We limit ourselves to the three-scale expansion (13). Since we have three different time scales T_0, T_1, and T_2, one has to modify the time derivatives as follows:

$$\frac{\mathrm{d}}{\mathrm{d}t} = \sum_{n=0}^{2} \varepsilon^n D_n, \quad D_n = \frac{\mathrm{d}}{\mathrm{d}T_n}. \tag{A1}$$

The equations governing μ_1, μ_2, and μ_3 are

$$D_0^2\mu_1 + \omega_0^2\mu_1 = 0, \tag{A2a}$$

$$D_0^2\mu_2 + \omega_0^2\mu_2 = -[k_1\mu_1^2 + k_{01}(D_0\mu_1)^2 + 2D_0D_1\mu_1], \tag{A2b}$$

$$D_0^2\mu_3 + \omega_0^2\mu_3 = -\Big\{k_2\mu_1^3 + D_1^2\mu_1 + \mu_1(2k_1\mu_2 + \\ + k_{02}(D_0\mu_1)^2) + 2[k_{01}D_0\mu_1(D_1\mu_1 + D_0\mu_2) + \\ + D_0D_2\mu_1 + D_0D_1\mu_2]\Big\} + h_3\sin(\omega_0T_0 + \omega_2T_2), \tag{A2c}$$

where we used the notations

$$k_{01} = \mathcal{M}_0\mu_0, \qquad k_{02} = \mathcal{M}_0^2(4+\mu_0^2),$$

$$k_1 = -\frac{4 - 9\mu_0^2 - \mu_0^4 + \varkappa\left(1-\mu_0^2\right)^2\left(4+3\mu_0^2\right)}{\mu_0\left(1-\mu_0^2\right)^2},$$

$$k_2 = -\frac{\mathcal{M}_0(12 - 27\mu_0^2 + 38\mu_0^4 + \mu_0^6) + 3\varkappa\left(1-\mu_0^2\right)^3}{3\mu_0^2\mathcal{M}_0\left(1-\mu_0^2\right)^3}.$$

The solution of Eq. (A2a) reads $\mu_1 = A(T_1,T_2)\times e^{i\omega_0T_0} + \\ + A^*(T_1,T_2)e^{-i\omega_0T_0}$. To prevent the secular terms in Eq. (A2b), one has to put $A(T_1,T_2) \equiv A(T_2)$; the same condition for Eq. (A2c) gives an equation for the oscillation amplitude of μ_1:

$$D_2A(T_2) + 4ic_1A^2A^* = -h_3\mathcal{M}_0c_2e^{i\omega_2T_2},$$

$$c_1 = \frac{5k_{01}k_1}{12\omega_0} - \frac{3k_2}{8\omega_0} + \frac{5k_1^2}{12\omega_0^3} + \frac{\omega_0}{24}\left(4k_{01}^2 - 3k_{02}\right), \tag{A3}$$

$$c_2 = \frac{1}{\mathcal{M}_0\omega_0}.$$

By solving Eq. (A3), one gets finally Eq. (14).

1. H.-B. Braun, Adv. in Phys. **61**, 1 (2012), http://www.tandfonline.com/doi/abs/10.1080/00018732.2012.663070.

2. A. Wachowiak, J. Wiebe, M. Bode, O. Pietzsch, M. Morgenstern, and R. Wiesendanger, Science **298**, 577 (2002), http://www.sciencemag.org/cgi/content/abstract/298/5593/577.
3. A. Hubert and R. Schäfer, *Magnetic Domains: the Analysis of Magnetic Microstructures* (Springer, Berlin, 1998).
4. S.-K. Kim, K.-S. Lee, Y.-S. Yu, and Y.-S. Choi, Appl. Phys. Lett. **92**, 022509 (2008).
5. Y.-S. Yu, H. Jung, K.-S. Lee, P. Fischer, and S.-K. Kim, Appl. Phys. Lett. **98**, 052507 (2011).
6. Y.B. Gaididei, V.P. Kravchuk, D.D. Sheka, and F.G. Mertens, Low Temp. Phys. **34**, 528 (2008).
7. V.P. Kravchuk, Y. Gaididei, and D.D. Sheka, Phys. Rev. B **80**, 100405 (2009).
8. Y. Gaididei, V.P. Kravchuk, D.D. Sheka, and F.G. Mertens, Phys. Rev. B **81**, 094431 (2010).
9. T. Okuno, K. Shigeto, T. Ono, K. Mibu, and T. Shinjo, J. Magn. Magn. Mater. **240**, 1 (2002).
10. A. Thiaville, J.M. Garcia, R. Dittrich, J. Miltat, and T. Schrefl, Phys. Rev. B **67**, 094410 (2003).
11. V. Kravchuk and D. Sheka, Phys. of Sol. State **49**, 1923 (2007).
12. L. Vila, M. Darques, A. Encinas, U. Ebels, J.-M. George, G. Faini, A. Thiaville, and L. Piraux, Phys. Rev. B **79**, 172410 (2009).
13. R. Wang and X. Dong, Appl. Phys. Lett. **100**, 082402 (2012).
14. M.-W. Yoo, J. Lee, and S.-K. Kim, Appl. Phys. Lett. **100**, 172413 (2012).
15. M. Abramowitz and I.A. Stegun, *Handbook of Mathematical Functions with Formulas, Graphs, and Mathematical Tables* (Dover, New York, 1964).
16. J. Kevorkian and J. Cole, *Perturbation Methods in Applied Mathematics* (Springer, Berlin, 1981).
17. A. Nayfeh, *Problems in Perturbation* (Wiley, New York, 1985).
18. A. Nayfeh, *Perturbation Methods* (Wiley, New York, 2008).
19. *The Object Oriented MicroMagnetic Framework*, note developed by M.J. Donahue and D. Porter mainly, from NIST. We used the 3D version of the 1.2α4 release, http://math.nist.gov/oommf/.
20. S. Petit-Watelot, J.-V. Kim, A. Ruotolo, R.M. Otxoa, K. Bouzehouane, J. Grollier, A. Vansteenkiste, B. Van de Wiele, V. Cros, and T. Devolder, Nat. Phys. **8**, 682 (2012).

Received 29.03.13

О.В. Пилиповський, Д.Д. Шека,
В.П. Кравчук, Ю.Б. Гайдідей, Ф.Г. Мертенс

МЕХАНІЗМ ШВИДКОГО
АКСІАЛЬНО СИМЕТРИЧНОГО ПЕРЕМИКАННЯ
ПОЛЯРНОСТІ МАГНІТНОГО ВИХОРУ

Р е з ю м е

Полярність магнітного вихору в наноточці може бути перемкнена під дією змінного магнітного поля, прикладеного перпендикулярно до осі наночастинки. В даній роботі запропоновано просту модель на основі колективних змінних, яка описує складну динаміку вихрового осердя, включаючи резонансну поведінку, слабконелінійний режим та динаміку перемикань. Передбачено наявність *хаотичної динаміки*. Всі аналітичні результати підтверджено мікромагнітними моделюваннями.

А.В. Пилиповский, Д.Д. Шека,
В.П. Кравчук, Ю.Б. Гайдидей, Ф.Г. Мертенс

МЕХАНИЗМ БЫСТРОГО
АКСИАЛЬНО СИММЕТРИЧНОГО ПЕРЕКЛЮЧЕНИЯ
ПОЛЯРНОСТИ МАГНИТНОГО ВИХРЯ

Р е з ю м е

Полярность магнитного вихря в наноточке может быть переключена под действием переменного магнитного поля, приложенного перпендикулярно оси наночастицы. В данной работе предложена простая модель на основе коллективных переменных, которая описывает сложную динамику вихревого сердечника, включая резонансное поведение, слабонелинейный режим и динамику переключений. Предусмотрено наличие *хаотической динамики*. Все аналитические результаты подтверждены микромагнитными моделированиями.

(*Продовження в наступному номері*)